

# 4<sup>th</sup> IFQMS

The 4th International Forum  
on Quantum Metrology and Sensing

## PROCEEDINGS

Short Presentations by Young Researchers  
Part 2: SE-03B

December 8th, 2021  
Online Conference (Zoom)

Joint Program Session with Quantum Innovation 2021



**Quantum Sensing Track : Short Presentations by Young Researchers****SE-03B. Short Presentations by Young Researchers on SE-02, 05 Topics [4th IFQMS]**

\*Note: Depending on the program, the order of presentations may change within the same group.

All the times in the program are Japan Standard time (GMT+9)

Dec 8 (Wed.)	Session / Presentation	Mentor Chair Co-chair / Presenter	Affiliation	Abstract ID
<b>13:10-14:30 SE-03B-01</b>				
	Mentor	Johnjoe McFadden	U Surrey	
	Mentor	Shigenori Tanaka	Kobe U	
	Mentor	Kiminori Maeda	Saitama U	
	Chair	Noriaki Yahata	QST	
	Co-chair	Akinari Yokoya	QST	
	Intracellular thermal conductivity determined by dual-functionalized diamond nanosensor	Madoka Suzuki	Osaka U	SE-03B-01-01
	Label-free analysis of diffusion constant in lipid bilayers using nanoscale diamond magnetometry	Hitoshi Ishiwata	QST	SE-03B-01-02
	Temperature sensing using silicon vacancy centers in detonation nanodiamonds	Masanori Fujiwara	Kyoto U	SE-03B-01-03
	Quantum-inspired machine learning for exponentially big neural data analysis	Kei Majima	QST	SE-03B-01-04
	Empirical verification of the violation of the temporal Bell inequality in bistable perception	Yasunori Aizawa	QST	SE-03B-01-05
	Tracking radiation damage induction pathway following core-hole creation of DNA molecules in aqueous solution	Yoshiaki Kumagai	TUAT	SE-03B-01-06
<b>14:50-16:10 SE-03B-02</b>				
	Mentor	Peter Hore	U Oxford	
	Mentor	Akihito Ishizaki	IMS	
	Mentor	Yasuteru Shigeta	U Tsukuba	
	Chair	Yoichi Takakusagi	QST	
	Co-chair	Tatsuhiko Imaoka	QST	
	High-resolution structure of an electron-transfer protein by neutron crystallography	Yuya Hanazono	TMDU	SE-03B-02-01
	Fabrication of a quantum sensor to reveal a topic in thermal physiology	Shuya Ishii	QST	SE-03B-02-02
	Investigation of irradiation induced nitrogen-vacancy centers in 5-nanometer-sized detonation nanodiamonds	Kit So	Kyoto U	SE-03B-02-03
	Formation of flavin anion and tyrosine radicals in avian Cryptochrome4	Hiroaki Otsuka	Waseda U	SE-03B-02-04
	Do neural activities of binocular rivalry follow a quantum probability model? A test of temporal Bell inequalities	Takahiro Hirao	QST	SE-03B-02-05
	X-ray absorption spectroscopy of a silicon phthalocyanine derivative, IR700, for X-ray excited photoimmunotherapy	Yudai Izumi	QST	SE-03B-02-06
	Magnetically sensitive radical pairs in avian cryptochrome 4 proteins	Jingjing Xu	U Oldenburg	SE-03B-02-07

## Intracellular thermal conductivity determined by dual-functionalized diamond nanosensor

Madoka Suzuki<sup>1</sup>

<sup>1</sup>*Institute for Protein Research, Osaka University*

*suzu\_mado@protein.osaka-u.ac.jp*

### Introduction

Cellular thermogenesis is an origin of rising body temperature. However, it is difficult to examine thermal effects in a small scale such as a cell or a nanoparticle. The difficulty is caused by a simple reason; i.e., the thermogenesis occurs within the volume of the heat source, while the heat escapes from its surface. When the size of a heat source (a fixed shape and volume is considered) decreases by half, the volume of the heat source becomes 1/8, whereas the surface area decreases only by 1/4. Therefore, as the scale of a system is reduced, the temperature rise can be orders of magnitude smaller and quicker than in larger systems such as a tissue and an organism. This difficulty has been eased recently by a variety of temperature nanoprobe and local heating methods. We can measure and manipulate temperature locally at the subcellular scale. Yet, the heat diffusion in cells, an essential knowledge to understand the results provided by those new methods, have never been determined experimentally [1]. In many cases, the heat diffusion in a cell has been considered as similar to that in cells.

### Method

Here, our recent study provided a new methodology to measure the thermal conductivity at the nanoscale [2]. The method utilizes a dual-functionalized diamond nanosensor that functions as both a nanothermometer and a nanoheater. We found that the thermal conductivity in HeLa and MCF-7 cell lines is surprisingly smaller (about 1/6) than in water. This new finding that the heat diffusion in a cell is significantly hindered than in water may suggest a new role of cellular thermogenesis in biology beyond the conventional understanding of rising body temperature. Now we can expect that larger or longer heat pulses are formed by metabolic processes in cells [3]. Intracellular signaling is a biochemical reactions caused by a diffusion of molecules. We propose that "thermal" signaling could also be a part of this intracellular process.

This work was supported by JSPS KAKENHI Grant No. 19H03198 and by the Human Frontier Science Program No. RGP0047/2018.

### References

- <sup>1</sup>M. Suzuki and T. Plakhotnik, *Biophysical Reviews*, 12, 593–600 (2020). doi: 10.1007/s12551-020-00683-8
- <sup>2</sup>S. Sotoma, C. Zhong, J.C.Y. Kah, H. Yamashita, T. Plakhotnik, Y. Harada and M. Suzuki, *Science Advances*, 7, eabd7888 (2021). doi: 10.1126/sciadv.abd7888
- <sup>3</sup>M. Suzuki and T. Plakhotnik, *Applied Physics Letters*, 119, 190502 (2021). doi: 10.1063/5.0063089

## Label-free analysis of diffusion constant in lipid bilayers using nanoscale diamond magnetometry

Hitoshi Ishiwata<sup>1</sup>, Hiroshi C. Watanabe<sup>2</sup>, Shinya Hanashima<sup>3</sup>,  
Takayuki Iwasaki<sup>4</sup>, Mutsuko Hatano<sup>4</sup>, Ryuji Igarashi<sup>1,5</sup>

<sup>1</sup>Institute for Quantum Life Science, National Institutes for Quantum and Radiological Science and Technology

<sup>2</sup>Quantum Computing Center, Keio University

<sup>3</sup>Department of Chemistry, Graduate School of Science, Osaka University

<sup>4</sup>Department of Electrical and Electronics Engineering, School of Engineering, Tokyo Institute of Technology

<sup>5</sup>PRESTO, Japan Science and Technology Agency

ishiwata.hitoshi@qst.go.jp

### Introduction

The NV center in a diamond is a quantum sensor with exceptional quality for highly sensitive nanoscale analysis of NMR spectra. In this study, we investigate diffusion constant of a lipid bilayer, a biological parameter that determines the dynamics of the lipid bilayer, utilizing ensemble-averaged nuclear spin detection from small volume  $\sim (6 \text{ nm})^3$ , which was determined by the depth of the NV center [1]. Observation of diffusion constant at different temperature reveals different phases of lipid bilayer [2]. The result builds foundation for label-free imaging of cell membranes for observation of phase composition and pristine dynamics that determines cellular functions.

### Result

In Figure 1, the result of the correlation spectroscopy was compared with the 2D molecular diffusion model constructed by Monte Carlo simulation combined with results from molecular dynamics simulation. There is a change in diffusion constant from  $1.5 \pm 0.25 \text{ nm}^2/\mu\text{s}$  to  $3.0 \pm 0.5 \text{ nm}^2/\mu\text{s}$  when the temperature changes from  $26.5 \text{ }^\circ\text{C}$  to  $36.0 \text{ }^\circ\text{C}$ . Observation of diffusion constant reveals different phases of lipid bilayer which identifies sub-compartment domains that are critical for cellular functions. In Figure 2, diffusion constant obtained from various different methods are shown. Previous results from Fluorescence Recovery After Photobleaching (FRAP) vary significantly depending on the selected markers as shown in Figure 2. Our results obtained from nanoscale diamond magnetometry are consistent with the results obtained from label-free bulk measurement using Magic-Angle Spinning Pulse Field Gradient NMR (MAS PFG NMR). Our method builds foundation for label-free imaging of cell membranes for observation of phase composition that determines cellular functions.

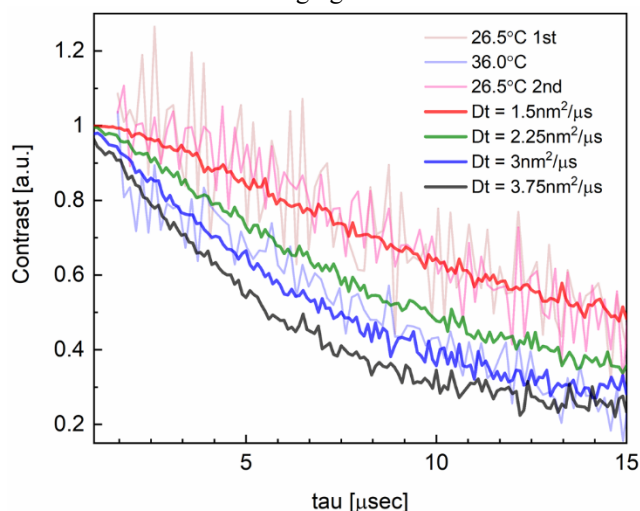


FIG. 1. Absolute value of correlation spectrum at  $26.5 \text{ }^\circ\text{C}$  (1st and 2nd) and  $36.0 \text{ }^\circ\text{C}$  are shown and compared with results of 2D molecular diffusion

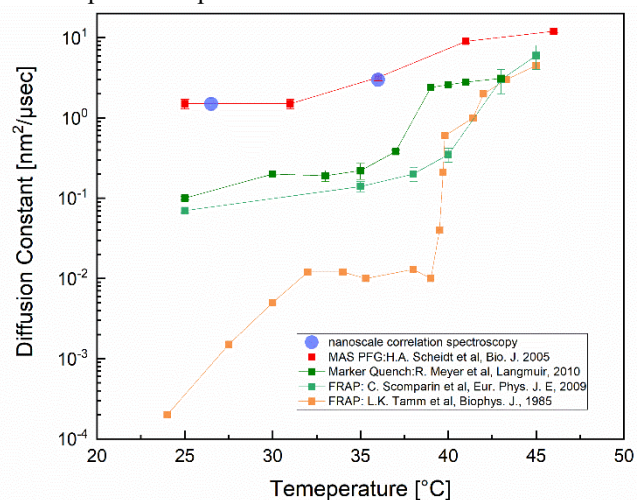


FIG. 2. Diffusion constant obtained from various measurement method compared with nanoscale correlation spectroscopy

### Reference:

<sup>1</sup>H. Ishiwata, et al, *APL*, 111, 043103 (2017). <sup>2</sup>H. Ishiwata, et al, *Adv. Quantum Technol.* 4, 2000106 (2021)

This research was supported by JST PRESTO Grant number JPMJPR17G1 and the MEXT Quantum Leap Flagship Program (MEXT Q-LEAP) Grant Number JPMXS0118067395, JPMXS0120330644.

## Temperature sensing using silicon-vacancy centers in detonation nanodiamonds

Masanori Fujiwara<sup>1</sup>, Gaku Uchida<sup>1</sup>, Izuru Ohki<sup>1</sup>, Ming Liu<sup>2</sup>, Akihiko Tsurui<sup>2</sup>, Taro Yoshikawa<sup>2</sup>, Masahiro Nishikawa<sup>2</sup>, and Norikazu Mizuochi<sup>1</sup>

<sup>1</sup>Institute for Chemical Research, Kyoto University, Gokasho, Uji, Kyoto 611-0011, Japan

<sup>2</sup>Business Development Center, Daicel Corporation, 1239, Shinzaike, Aboshi-Ku, Himeji, Hyogo

671-1283, Japan

masafuji@scl.kyoto-u.ac.jp

### Introduction

Nanodiamonds containing silicon-vacancy centers (SiV-NDs) are promising candidates for all-optical nanoscale thermometry. For the practical application of SiV-NDs into a biological system like a living cell, NDs smaller than 30 nm are suitable to pass through their membrane with minor damage. However, since the particle size of SiV-NDs reported for temperature sensing is larger than 200 nm<sup>1</sup>, it is difficult to introduce such NDs into the target position without invasive and complicated methods. As one of the efforts to overcome this problem, we developed SiV containing NDs via detonation process (SiV-DNDs)<sup>2</sup> since the detonation method can create small-size and massive NDs at a low cost. In this presentation, we show the photoluminescence (PL) spectral response to the temperature of SiV-DNDs.

### Method

We first prepared polyglycerol-coated SiV-DNDs after purification and dispersion processes. The particle size of SiV-DNDs is distributed at around 20 nm judging from the size histogram of 208 DNDs selected from a transmission electron microscope (TEM) image as shown in Fig. 1(a). The particle size of the DNDs is small enough to use inside the cell. We next prepared the SiV-DND suspension, dropped them on a coverslip, and dried them in ambient conditions. We observed the PL image and spectrum by a homebuilt confocal microscope with a thermoplate to control the sample temperature. From the confocal image, we found several bright spots (SiV-DND's aggregations) with the SiV center's zero phonon line (ZPL) at a wavelength of 737 nm. Figure 1(b) shows ZPL peak wavelength ( $\lambda_p$ ) as a function of the sample temperature for a bright spot. We confirmed the  $\lambda_p$  linearly red-shifted with increasing temperature ranging from 22 °C to 40.5 °C. The peak wavelength sensitivity to temperature ( $\Delta\lambda/\Delta T$ ) is 0.015 nm K<sup>-1</sup>, which agrees with the result of SiV center's ensemble in a diamond substrate (0.0124 nm K<sup>-1</sup>)<sup>1</sup>. Using  $\Delta\lambda/\Delta T$ , we evaluated the temperature sensitivity  $\eta_T$ , which is defined the uncertainty  $\sigma_T$  at a unit measurement time  $t_{\text{int}}$  (Fig. 1c). We found a bright spot with  $\eta_T = 1.1 \text{ K}/\sqrt{\text{Hz}}$ , which indicates sub-Kelvin precision was realized for 10 s integration time. All-optical thermometers such as small nanoparticles will be a key factor for thermometry of nanosystems like organelle in the living cell.

This work was supported by MEXT Q-LEAP No. JPMXS0120330644.

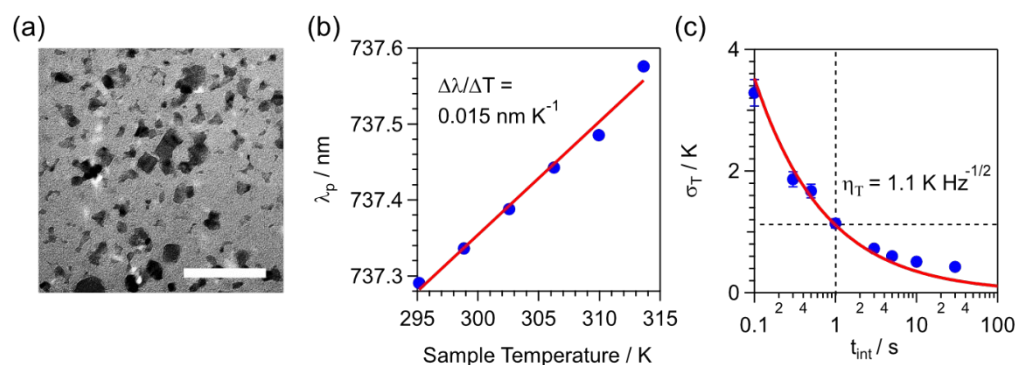


**Figure 1** (a) TEM image of SiV-DNDs. Scale bar indicates 100 nm. (b) ZPL peak wavelength ( $\lambda_p$ ) as a function of the sample temperature for a bright spot (SiV-DNDs' aggregation) selected from a confocal image. The peak sensitivity to temperature ( $\Delta\lambda/\Delta T$ ) was obtained by a line fit from the experimental data (filled circles). (c) Temperature uncertainty ( $\sigma_T$ ) of the spot as a function of measurement time  $t_{\text{int}}$ . The experimental data (filled circles) are fitted on a curve  $\propto 1/\sqrt{t_{\text{int}}}$ .

### Reference

<sup>1</sup>C. T. Nguyen, et al., *Appl. Phys. Lett.*, **112**, 203102 (2018).

<sup>2</sup>Y. Makino, et al., *Diam. Relat. Mater.*, **112**, 108248 (2021).

# Quantum-inspired machine learning for exponentially big neural data analysis

Kei Majima<sup>1,2</sup>

<sup>1</sup>*Institute for Quantum Life Science, National Institutes for Quantum Science and Technology (QST), Chiba, Japan*

<sup>2</sup>*PRESTO, Japan Science and Technology Agency (JST), Japan*

*majima.kei@qst.go.jp*

## Introduction

Machine learning algorithms specialized for neural data have allowed the extraction of information encoded in the brain. As an example, in previous studies, the images human subjects see were reconstructed from their brain activity measured via functional magnetic resonance imaging (fMRI) [1]. However, the application of those machine learning algorithms to high-resolution fMRI data, which may become mainstream in the near future, is limited due to their high computational cost. To solve this problem, scalable machine learning algorithms are being designed by utilizing computational techniques developed in the field of quantum computation [2,3]. In this report, taking one of the popular statistical methods, principal component analysis (PCA), as an example, we show that machine algorithms can be approximated with the use of such quantum-inspired techniques. The computational time and approximation performance of quantum-inspired PCA are demonstrated. The main results of this report have been presented in a previous paper by the author [3].

## Methods

In this report, the computational time and performance were compared between quantum-inspired PCA and its exact counterpart (*i.e.*, exact PCA). Due to space limitations, the details of the algorithms and datasets used are omitted in this report; however, they have been explained in the previous study [3]. Briefly, the computational times of the two algorithms were measured by applying them to simulation data. To characterize the dependence on the input dimensionality, the number of input dimensions in the simulation data was systematically changed. The performances of those two algorithms were evaluated by applying them to five benchmark datasets, and the variance explained by the top 100 PCs was measured and used as a performance metric in this report.

## Results

Both the computational time and performance (*i.e.*, explained variance) are shown in Figure 1. Results show that quantum-inspired PCA was significantly faster than the exact PCA, and its performance was maximally 7% worse than the exact PCA for these five datasets.

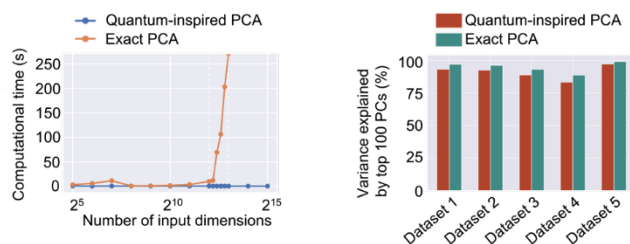


FIG 1. Comparison of the computational time and performance between quantum-inspired PCA and its exact counterpart.

## Discussion and Conclusions

In this report, quantum-inspired PCA was applied to simulation and real benchmark datasets, and its computational time and performance were compared with those of the exact PCA. As results, quantum-inspired PCA was significantly faster than its exact counterpart, and it showed moderate approximation performance on the five datasets. These results suggest a possibility that high-dimensional neural data whose size is intractable with previous machine learning algorithms can be efficiently analyzed using such quantum-inspired algorithms.

## References

- <sup>1</sup>G. Shen, T. Horikawa, K. Majima, Y. Kamitani, *PLOS Computational Biology*, Volume **15**, e1006633 (2019).
- <sup>2</sup>E. Tang, *Physical Review Letters*, Volume **127**, 060503 (2021).
- <sup>3</sup>N. Koide-Majima, K. Majima, *Neural Networks*, Volume **135**, 55–67 (2021).

This research was supported by MEXT Q-LEAP (JPMXS0120330644), JSPS KAKENHI (20K16465), JST ERATO (JPMJER1801), and JST PRESTO (JPMJPR2128).

## Empirical verification of the violation of the temporal Bell inequality in bistable perception

Yasunori Aizawa<sup>1,2</sup>, Naotsugu Tsuchiya<sup>3</sup>, Emmanuel Pothos<sup>4</sup>, Jerome Busemeyer<sup>5</sup>, Peter Bruza<sup>6</sup>,  
and Makiko Yamada<sup>1,7</sup>

<sup>1</sup>*Institute for Quantum Life Science, National Institutes for Quantum Science and Technology*

<sup>2</sup>*Graduate School of Medicine, Tohoku University*

<sup>3</sup>*School of Psychological Sciences, Monash University*

<sup>4</sup>*School of Arts and Social Sciences, Department of Psychology, City, University of London*

<sup>5</sup>*Department of Psychological and Brain Sciences, Indiana University Bloomington*

<sup>6</sup>*Faculty of Science and Technology, Queensland University of Technology*

<sup>7</sup>*Institute for Quantum Medical Science, National Institutes for Quantum Science and Technology*  
aizawa.yasunori@qst.go.jp

### Introduction

The purpose of the present study is to investigate quantum-like properties of mental states in bistable perception. In order to do this, we tested whether the temporal Bell inequality applied to bistable perception experiments[1] can be violated. In the present study, we used visual stimuli [2], where we can continuously and systematically manipulate two types of ambiguities in the perceived rotation of dots. When the rotation angle is large, the stimuli induce bistable percept. When the angle is small, the direction of rotation of the stimuli becomes difficult to judge. We use the stimuli to test if the temporal Bell inequality can be violated, and if so, under what parameter regime, it can be violated.

### Method

Two patterns were presented alternately: a visual stimulus consisting of four disks, and one in which the disks were rotated by a specific angle (5-45 degrees) in each trial [FIG. 1(A)]. When the angle of rotation was close to 45 degrees, stimuli were perceived to rotate in one of the two directions for a while with occasional reversals at random times (i.e., bistable perception). When the angle of rotation was close to 5 degrees, no rotation was perceived beyond the angle of rotation of the stimulus, and left and right rotations were perceived alternately, but the angle of rotation was so small that it was difficult to determine the direction of rotation [FIG. 1(B)]. At two time points after the beep, the participants responded by pressing a button in the direction of rotation that they saw at that time [FIG. 1(C)].

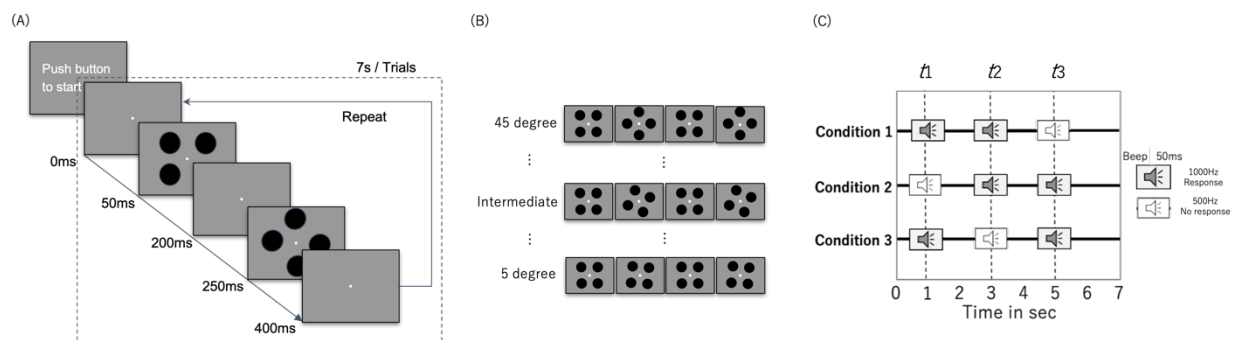


FIG. 1. (A) Schematic illustration of the task. (B) A set of rotation angles (5-45 degrees in 5 degree steps). (C) Three timings on the measurement of perceived stimuli. The perceived rotation direction was measured at two out of three timepoints for the calculation of the temporal Bell inequality.

### Reference

<sup>1</sup>H. Atmanspacher, and T. Filk, *J. Math. Psychol.* **54**, 314-321 (2010).

<sup>2</sup>S. Takei and S. Nishida, *J. Vision.* **10**, 23 (2010).

<sup>3</sup>M. M. Wilde and A. Mizel, *Found. Phys.* **42**, 256 (2012).

### Acknowledgement

This work was supported by JSPS KAKENHI JP20H05711 and MEXT Q-LEAP Grant Number JPMXS0120330644.

## Tracking radiation damage induction pathway following core-hole creation of DNA molecules in aqueous solution

Yoshiaki Kumagai<sup>1,2</sup>, Masatoshi Ukai<sup>1,2</sup>, Akinari Yokoya<sup>3</sup>

<sup>1</sup>*Department of Applied Physics, Tokyo University of Agriculture and Technology*

<sup>2</sup>*Institute of Engineering, Tokyo University of Agriculture and Technology*

<sup>3</sup>*Institute for Quantum Life Science, National Institute for Quantum Science and Technology*

kumagai@go.tuat.ac.jp

### Introduction

Ionizing radiation often causes irreversible DNA damage in a living cell of tissue and the mutation or cell death are thought to arise from localization of damage known as a clustered DNA damage site [1]. Recently, it is recognized that the production of the DNA molecules with inner-shell vacancies after irradiation can be a cause of clustered DNA damages [2]. We have reported the x-ray absorption near-edge structure (XANES) spectra at photon energies near the nitrogen K-shell ionization potential of the base moieties of aqueous nucleotides [3]. The measuring excitation energies and binding energies of the electrons in the nitrogen K-shell orbitals at different pH conditions predicted the hydration interaction of bases in nucleotides with hydrated water molecules. This hydration interaction has been further confirmed by the spectroscopy of the secondary and Auger electrons [4] (FIG.1). These findings gave rise to a possible deposition of excess charge from doubly ionized DNA to water molecules, which may suppress the clustered DNA damage induction. We studied the reaction pathways and dynamics of core-hole DNA molecules in the aqueous solution with their identified electronic states toward chemically stable and irreparable damages.

### Results

We used monochromatic soft x-rays at SPring-8 BL23SU to selectively excite or ionize an inner shell electron of a specific atom in aqueous nucleotide molecules, which have been introduced into the vacuum using a liquid micro-jet technique. In order to track the chemical reaction sequences following initial core-hole states created by the primary radiations, we have focused on particular events by excitation and to probe outgoing luminescences [5]. This is a nondestructive analysis of the excited intermediate species produced in a molecular reaction on the damage induction pathway. We obtained the first evidence of luminescence spectra of aqueous uridine-5'-monophosphate (UMP) after x-ray absorption (FIG.2). The cause of luminescence can be due to the parent species produced following the double ionization of aqueous UMP, and emission of excess positive charge and excess internal energy from double charged UMP.

We also established the mass spectroscopy for the secondary ion fragments produced via the relaxation of core-hole nucleotide molecules in aqueous solution which extended the adaptabilities of the soft x-ray spectroscopy for the DNA damaging using a liquid-jet technique.

### Acknowledgement

This work was supported by JSPS KAKENHI (Grant Nos. 20H04338).

### Reference

- <sup>1</sup>D. Goodhead, *Int. J. Radiat. Bio.*, **65**, 7 (1994).
- <sup>2</sup>A. Yokoya *et al.*, in *Charged Particle and Photon Interaction with Matter*, (CRC Press: Boca Raton, 2011), pp.543-574.
- <sup>3</sup>H. Shimada *et al.*, *Chem. Phys. Lett.*, **591**, 137 (2014); H. Shimada *et al.*, *J. Chem. Phys.*, **141**, 055102 (2014); H. Shimada *et al.*, *J. Chem. Phys.*, **142**, 175102 (2015).
- <sup>4</sup>Y. Takeda *et al.*, *Quantum Beam Sci.*, **4**, 10 (2020)
- <sup>5</sup>Y. Terao *et al.*, *Int. J. Radiat. Bio.*, (published online; 2021)

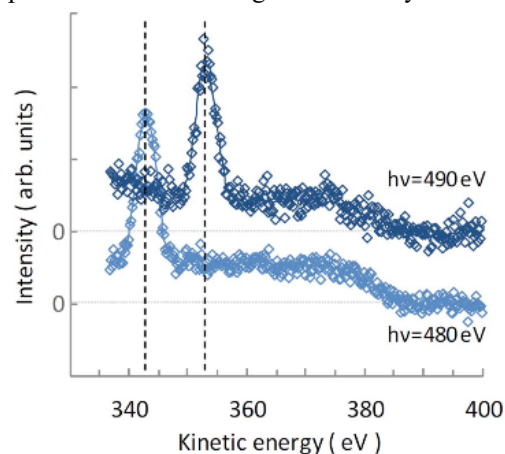


FIG. 1. Electron kinetic energy spectra for aqueous UMP at pH = 7.5 at the x-ray photon energies of 480 eV and 490 eV [4].

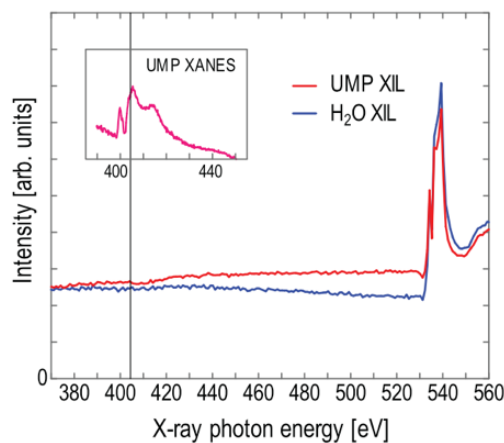


FIG. 2. Yields of x-ray induced luminescence for aqueous UMP and pure water as a function of x-ray photon energy [5]. The inset shows the XANES spectra for aqueous UMP.

## High-resolution structure of an electron-transfer protein by neutron crystallography

Yuya Hanazono<sup>1,2,3</sup>, Yu Hirano<sup>2,4</sup>, Kazuki Takeda<sup>1</sup>, Katsuhiko Kusaka<sup>5</sup>, Taro Tamada<sup>2</sup>, and Kunio Miki<sup>1</sup>

<sup>1</sup>*Department of Chemistry, Graduate School of Science, Kyoto University*

<sup>2</sup>*Institute for Quantum Life Science, National Institutes for Quantum Science and Technology*

<sup>3</sup>*Medical Research Institute, Tokyo Medical and Dental University*

<sup>4</sup>*PRESTO, Japan Science and Technology Agency*

<sup>5</sup>*Frontier Research Center for Applied Atomic Sciences, Ibaraki University*

hanazono.str@tmd.ac.jp

### Introduction

High-potential iron-sulfur protein (HiPIP) is a component of electron transfer from cytochrome *bc*<sub>1</sub> complex to light-harvesting-reaction center complexes (LH1-RC) in bacterial photosynthesis. HiPIP possesses a cubane-like Fe<sub>4</sub>S<sub>4</sub> cluster at its center with a redox potential of above +300 mV. This high potential arises from the hydrogen bonds and hydrophobic environment around the iron-sulfur cluster [1–3]. In order to clarify the effect of hydrogen bond on the redox potential and reaction mechanism, we determined the neutron structure of HiPIP and obtained the precise locations of the hydrogen nuclei.

### Methods

We collected X-ray and neutron diffraction data of oxidized HiPIP at 0.66 and 1.2 Å resolution, respectively, from the same crystal at a cryogenic temperature of 100 K. The initial refinement of X-ray data was performed at 1.2 Å resolution. Then, the refinements with anisotropic atomic displacement parameters were performed at 0.66 Å resolution. After that, the joint refinement of neutron and X-ray data was performed. The amide protons that had occupancies more than or equal to 0.60 that of deuterium or 0.75 that of protium and the deuterium atoms of the side chains in a single conformation were refined without geometry restraints.

### Results

In the case of the NH...O hydrogen bond, most of the nucleus positions of the amide protons shift toward the acceptor atoms. These hydrogen atoms are attracted by the electrostatic force. On the other hand, some hydrogen atoms point away from the acceptor atoms. Around these hydrogen atoms, there is another oxygen atom nearby that can form a hydrogen bond. Generally, the planarity of the peptide bond is discussed based on  $\omega$ -angles due to the insufficient structural data for the amide protons. In this study, we focus on the planarity of the H<sub>i</sub>-N<sub>i</sub>-C<sub>i-1</sub>=O<sub>i-1</sub> planes, where *i* represents the residue number, in the peptide bond. To evaluate the planarity of peptide bonds including hydrogen atoms, the positions of hydrogen atoms and oxygen atoms are defined with the in-plane angle ( $\gamma_H$ ,  $\gamma_O$ ), the out-of-plane angle with the C<sub>i-1</sub>-N<sub>i</sub>-C<sub>ai</sub> plane ( $\delta_H$ ,  $\delta_O$ ). There is a substantial correlation between  $\delta_H$  and  $\delta_O$ . When the amide protons deviate from the peptide plane owing to the electrostatic interaction, the position of the oxygen atoms of previous residues shifts in the opposite direction. Consequently, the planarity of the H<sub>i</sub>-N<sub>i</sub>-C<sub>i-1</sub>=O<sub>i-1</sub> planes is mainly preserved. Moreover, the orientation of the amide proton of Cys75 is different in the reduced and oxidized states possibly due to the electron storage capacity of the iron-sulfur cluster. The change in the electron storage capacity will facilitate the electron transfer from HiPIP to LH1-RC.

### References

- <sup>1</sup>T. Glaser *et al.*, Schmitt, *J. Am. Chem. Soc.*, **123**, 4859–4860 (2001).
- <sup>2</sup>S. Niu *et al.*, *J. Am. Chem. Soc.*, **131**, 5724–5725 (2009).
- <sup>3</sup>A. Dey *et al.*, *Science*, **318**, 1464–1468 (2007).

### Acknowledgements

This work was supported by the Photon and Quantum Basic Research Coordinated Development Program, Quantum Leap Flagship Program (Q-LEAP) JPMXS0120330644 from the Ministry of Education, Culture, Sports, Science and Technology (MEXT), PRESTO JPMJPR17G7 from the Japan Science and Technology Agency (JST), and Grants-in-Aid for Scientific Research (C) JP20K06523, for Research Activity Start-up JP25891030 and JP20K22642 and for Young Scientists (B) JP15K18494 from the Japan Society for the Promotion of Science (JSPS).

## Fabrication of a quantum sensor to reveal a topic in thermal physiology

Shuya Ishii<sup>1,2</sup>

<sup>1</sup>*Takasaki Advanced Radiation Research Institute, National Institutes for Quantum Science and Technology, 1233 Watanuki, Takasaki, Gunma 370-1292, Japan*

<sup>2</sup>*Institute for Quantum Life Science, National Institutes for Quantum Science and Technology, 4-9-1 Ana-gawa, Inage-ku, Chiba 263-8555, Japan*

### Abstract

At first, I'll talking about a topic of thermal physiology in myocardial contraction to introduce the importance of focusing on temperature in biological viewpoint. During excitation-contraction coupling of striated muscle, sarcomeres are activated via thin filament structural changes, i.e., from the "off" state to the "on" state, in response to a rise in the intracellular  $\text{Ca}^{2+}$  concentration. We systematically investigated the effects of rapid heating by infra-red (IR) laser irradiation on the sliding of thin filaments reconstituted with human cardiac  $\alpha$ -tropomyosin (Tm) and bovine ventricular troponin (Tn), or rabbit fast skeletal Tm-Tn complex in the *in vitro* motility assay. The findings in our studies suggest that the "on-off" equilibrium of the cardiac thin filament state is partially shifted toward the "on" state in diastole at the body temperature, enabling rapid and efficient myocardial dynamics in systole [1,2].

Next, I'll show you a study of fabricating a quantum sensor (under submission), which has been getting a lot of attention in biological field. Negatively charged nitrogen-vacancy ( $\text{NV}^-$ ) center in diamond is known as quantum sensor, can be used to measure small changes in physical quantities, such as temperature [3]. Electron beam irradiation into type-Ib diamond is known as a good method for the creation of high concentration negatively-charged nitrogen-vacancy ( $\text{NV}^-$ ) centers by which highly sensitive quantum sensors can be fabricated. In order to understand the creation mechanism of  $\text{NV}^-$  centers, we study the behavior of substitutional isolated nitrogen (P1 centers) and  $\text{NV}^-$  centers in type-Ib diamond, with an initial P1 concentration of 40-80 ppm by electron beam irradiation up to  $8.0 \times 10^{18}$  electrons/cm<sup>2</sup>. P1 concentration and  $\text{NV}^-$  concentration were measured using electron spin resonance and photoluminescence measurements. Comparing concentration of P1 centers with that of  $\text{NV}^-$  centers, it suggests that a part of P1 centers plays a role in the formation of other defects. The usefulness of electron beam irradiation to type-Ib diamonds was confirmed by the resultant conversion efficiency from P1 to  $\text{NV}^-$  center around 12-19%. The result obtained in this study is useful to understand the creation mechanism of  $\text{NV}^-$  centers, leading to realize highly sensitive quantum sensors.

### Acknowledgement

This work was supported by Quantum Leap Flagship Program (Q-LEAP; JPMXS 0118067395) of MEXT.

### Reference

1. Oyama K, Mizuno A, Shintani SA, Itoh H, Serizawa T, Fukuda N, et al. Microscopic heat pulses induce contraction of cardiomyocytes without calcium transients. *Biochem Biophys Res Commun* [Internet]. 2012;417(1):607–12. Available from: <http://dx.doi.org/10.1016/j.bbrc.2011.12.015>
2. Ishii S, Oyama K, Arai T, Itoh H, Shintani SA, Suzuki M, et al. Microscopic heat pulses activate cardiac thin filaments. *J Gen Physiol*. 2019;151(6):860–9.
3. Barry JF, Schloss JM, Bauch E, Turner MJ, Hart CA, Pham LM, et al. Sensitivity optimization for  $\text{NV}^-$ -diamond magnetometry. *Rev Mod Phys*. 2020;92(1):015004(68).

## Investigation of irradiation induced nitrogen-vacancy centers in 5-nanometer-sized Detonation nanodiamonds

Frederick T.-K. So<sup>1,2,3</sup>, Alexander I. Shames<sup>4</sup>, Daiki Terada<sup>2,3</sup>, Takuya Genjo<sup>2,3</sup>, Hiroki Morishita<sup>1</sup>, Izuru Ohki<sup>1</sup>, Takeshi Ohshima<sup>5</sup>, Shinobu Onoda<sup>5</sup>, Hideaki Takashima<sup>6</sup>, Shigeki Takeuchi<sup>6</sup>, Norikazu Mizuochi<sup>1</sup>, Ryuji Igarashi<sup>3,7</sup>, Masahiro Shirakawa<sup>2,3\*</sup>, Takuya F. Segawa<sup>2,8\*</sup>

<sup>1</sup>Institute for Chemical Research, Kyoto University

<sup>2</sup>Department of Molecular Engineering, Graduate School of Engineering, Kyoto University

<sup>3</sup>Institute for Quantum Life Science, National Institutes for Quantum and Radiological Science and Technology

<sup>4</sup>Department of Physics, Ben-Gurion University of the Negev, Israel

<sup>5</sup>Takasaki Advanced Radiation Research Institute, National Institutes for Quantum Science and Technology

<sup>6</sup>Department of Electronic Science and Engineering, Kyoto University

<sup>7</sup>National Institute for Radiological Sciences, National Institutes for Quantum Science and Technology

<sup>8</sup>Laboratory for Solid State Physics, ETH Zurich, Switzerland

so.kit.58a@st.kyoto-u.ac.jp

### Introduction

Nanodiamonds containing negatively-charged Nitrogen-Vacancy (NV<sup>-</sup>) centers are versatile room-temperature quantum sensors in a growing field of research. Yet, knowledge regarding the formation mechanism in very small particles is still limited. Here, the study was focused on the formation of the smallest NV<sup>-</sup>-containing diamonds, 5 nm detonation nanodiamonds (DNDs). As a reliable method to quantify NV<sup>-</sup> centers in nanodiamonds, half-field signals in electron paramagnetic resonance (EPR) spectroscopy are recorded. By comparing the NV<sup>-</sup> concentration in a series of nanodiamonds (5 - 100 nm), it was shown that the formation process in DNDs is unique in several aspects. NV<sup>-</sup> centers in DNDs are already formed during electron irradiation, without the need for high-temperature annealing. The effect was interpreted in terms of “self-annealing”, where size and type dependent effects enable vacancy migration at lower temperature. Although NV<sup>-</sup> concentration increases with particle size, the NV<sup>-</sup> concentration in NDs surpasses that of 20 nm-sized nanodiamonds. Using Monte-Carlo simulations, we show that the higher substitutional Nitrogen concentration compensates the vacancy loss induced by the large particle surface. Upon  $1.5 \times 10^{19}$  e<sup>-</sup>/cm<sup>2</sup> electron irradiation, DNDs show a 12.5-fold NV<sup>-</sup> increment with no sign of saturation. These findings can be of interest for the creation of defects in other very small semiconductor nanoparticles.

This work was supported by MEXT Q-LEAP Grant Number JPMXS0120330644 & JPMXS0118067395, KAKENHI (Grants 20H00453, 18K19297)

### Method

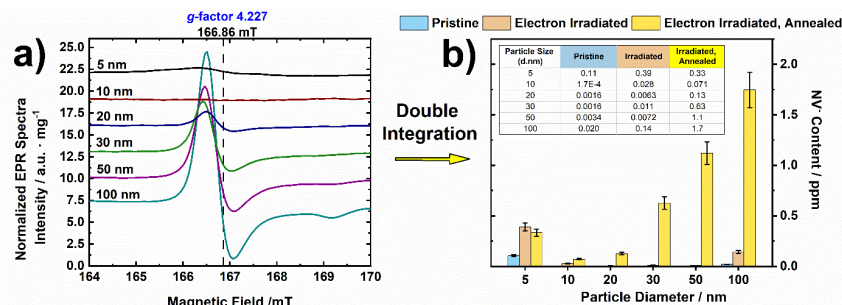


Figure 1. (a) Continuous-wave half-field EPR spectra of electron-irradiated (2 MeV,  $5 \times 10^{18}$  e<sup>-</sup>/cm<sup>2</sup>) nanodiamonds with different particle size after high-temperature annealing. The double integral of the signal at  $g_{\text{eff}} = 4.227$  provides the NV<sup>-</sup> concentration. (b) A summary graph of NV<sup>-</sup> content (ppm, in units of atomic ratio) in NDs of different sizes, measured via the half-field EPR technique. Blue bars are the pristine nanodiamonds; Orange bars are the electron-irradiated nanodiamonds; Yellow bars are the electron-irradiated and subsequently annealed nanodiamonds (derived from the  $g_{\text{eff}} = 4.227$  signal in the EPR spectrum of Fig. 1(a)). Electron irradiation was conducted with 2 MeV electrons at a fluence of  $5 \times 10^{18}$  e<sup>-</sup>/cm<sup>2</sup>; Annealing was performed at 800 °C in vacuum for 2 h. All samples were boiling acid treated to remove Fe<sup>3+</sup> impurities, which overlap with the half-field EPR NV<sup>-</sup> signal. Inset table shows the corresponding NV<sup>-</sup> concentrations in ppm. Errors in NV<sup>-</sup> concentration do not exceed  $\pm 15\%$ .

## Formation of flavin anion and tyrosine radicals in avian Cryptochrome4

Hiroaki Otsuka<sup>1</sup>, Hiromasa Mitsui<sup>1</sup>, Kota Miura<sup>1</sup>, Keiko Okano<sup>1</sup>, Yasushi Imamoto<sup>2</sup>, Toshiyuki Okano<sup>1</sup>

<sup>1</sup>Department of Electrical Engineering and Bioscience, School of Advanced Science and Engineering,  
Waseda University

<sup>2</sup>Department of Biophysics, Graduate School of Science, Kyoto University  
o1.2t5.8tt21.tf@ruri.waseda.jp

### Introduction

Many animals, such as avian and insects, exhibit light-dependent magnetoreception [1] that is likely mediated by the magnetic field-dependent chemical reaction of a pair of entangled radicals, called radical pair mechanism (RPM) [2].

Avian CRY4 is a plausible magnetoreceptor operating through RPM (FIG. 1) in the retina [3,4]. Our previous study suggested that chicken CRY4 (cCRY4) changes its conformation upon blue light irradiation [4] along with the formation of neutral radical FAD (FADH<sup>•</sup>) [5]. Together with the retinal localization of CRY4, it is a leading candidate of magnetoreceptor in birds. Therefore, analysis of the molecular changes after photoreception by CRY4 will be a key step for elucidation of RPM in the magnetoreception.

In this study, we measured the transient reactions up to the formation of FADH<sup>•</sup> after photoreception of CRY4 by millisecond timescale spectroscopy. Singular value decomposition (SVD) was applied to detailed analysis of the photoreactions. For comparative analysis, the recombinant CRY4 of magnetically migrating European robin (ErCRY4) was prepared.

### Method

Recombinant cCRY4 samples were purified by GST-tag purification system. Transient reactions of each sample were measured by laboratory-built, time-resolved spectrophotometry system. Obtained data were decomposed by SVD analysis and reconstructed into the spectra of each independent reaction (B spectra). SVD analysis yielded the spectrum representing steady state difference spectrum (B0 spectrum) and the two spectra representing the spectral changes occurring up to steady state (B1 and B2 spectra).

### Results and discussion

Regardless of the presence of dithiothreitol (DTT), flavin anion radical (FAD<sup>•-</sup>), a precursor of FADH<sup>•</sup>, was formed just after the blue light irradiation of ground state of cCRY4 and ErCRY4 (having oxidized FAD: FAD<sub>OX</sub>). FAD<sup>•-</sup> was then protonated to FADH<sup>•</sup> on the time scale of sub-seconds. In the absence of DTT, FAD<sup>•-</sup> was oxidized to FAD<sub>OX</sub> more rapidly than the protonation.

The spectral data were decomposed to three difference spectra (B0–B2) by SVD, representing two independent reactions; the oxidation and protonation. Time constants for the protonation from FAD<sup>•-</sup> to FADH<sup>•</sup> and the oxidation from FAD<sup>•-</sup> to FAD<sub>OX</sub> was 200 ms and 34 ms, respectively. Such a large difference in the time constants between the oxidation and protonation suggests the bifurcation of FAD<sup>•-</sup> bound to cCRY4 and ErCRY4. Furthermore, the presence of tyrosine neutral radical (Tyr-O<sup>•</sup>) was suggested by the spectrum for FAD<sup>•-</sup> oxidation in cCRY4. Based on these results, we speculate that FAD<sup>•-</sup> could be paired with Tyr-O<sup>•</sup>, and that magnetoreception may be achieved by detecting the ratio of the state of entangled [FAD<sup>•-</sup> Tyr-O<sup>•</sup>]. A comparison of photoreactions in cCRY4 and ErCRY4 would allow us to consider the differences in magnetoreception mechanisms between nesting and migrating birds.

### Reference

<sup>1</sup>R. Wiltschko and W. Wiltschko, *Sens. Nat.* **739**, 126 (2012); <sup>2</sup>T. Ritz, S. Adem, and K. Schulten, *Biophys. J.* **78**, 707 (2000); <sup>3</sup>Y. Kubo, M. Akiyama, Y. Fukada, and T. Okano, *J. Neurochem.* **97**, 1155 (2006); <sup>4</sup>R. Watari, C. Yamaguchi, W. Zemba, Y. Kubo, K. Okano, and T. Okano, *J. Biol. Chem.* **287**, 42634 (2012); <sup>5</sup>H. Mitsui, T. Maeda, C. Yamaguchi, Y. Tsuji, R. Watari, Y. Kubo, K. Okano, and T. Okano, *Biochemistry* **54**, 1908 (2015).

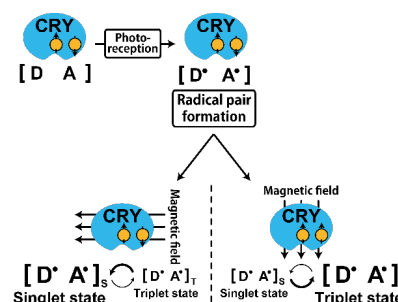


FIG. 1. Radical pair model mediated by cryptochrome CRYs photoactivation followed by formation of two entangled radicals are assumed to detect the geomagnetic field.

## Do neural activities of binocular rivalry follow a quantum probability model? A test of temporal Bell inequalities

Takahiro Hirao<sup>1,2</sup>, Naotsugu Tsuchiya<sup>3</sup>, Emmanuel Pothos<sup>4</sup>, Jerome Busemeyer<sup>5</sup>, Peter Bruza<sup>6</sup>, and Makiko Yamada<sup>1,2</sup>

<sup>1</sup>*Institute for Quantum Life Science, National Institutes for Quantum Science and Technology*

<sup>2</sup>*Institute for Quantum Medical Science, National Institutes for Quantum Science and Technology*

<sup>3</sup>*School of Psychological Sciences, Monash University*

<sup>4</sup>*School of Arts and Social Sciences, Department of Psychology, City, University of London*

<sup>5</sup>*Department of Psychological and Brain Sciences, Indiana University Bloomington*

<sup>6</sup>*Faculty of Science and Technology, Queensland University of Technology*

hirao.takahiro@qst.go.jp

### Introduction

Binocular rivalry refers to a phenomenon in which the perceived image changes spontaneously over time when the two eyes are presented with different images. The purpose of this study is to test whether the violation of temporal Bell inequality can be experimentally observed in binocular rivalry. If the temporal Bell inequality is violated (under no-signaling in time: NSIT), it implies that the perception of the rival stimuli cannot be assumed to be definite at each point in time (i.e., “realism” in the corresponding mental representations is violated), which is a key indication of non-classical behavior (as in, for example, quantum-like systems) [1]. Here, to test the violation of the inequality, we used binocular rivalry and measured both subjective reports and electroencephalogram (EEG). With EEG, we used frequency-tagging technique to track the cortical signal driven by each eye’s stimulus, known as the steady-state visual evoked potential (SSVEP). We present the conceptual and methodological approaches to test the temporal Bell inequality.

### Method

Two checkerboards flickering at different frequencies (red stimulus at 7.5 Hz; blue stimulus at 6.6 Hz) were dichoptically presented, one to each eye [FIG. 1(A) (B)]. Participants were asked to report their perception of the rival stimuli at two out of three different timepoints [FIG. 1(C)]. The electroencephalogram (EEG) was recorded from 28 scalp sites at a sampling rate of 1000 Hz. The EEG was re-referenced to the averaged mastoids and band-pass filtered with a 0.1-50 Hz cutoff. The prominent artifacts were identified and removed by the individual component analysis. The SSVEP signals were extracted by using an adaptive recursive least-square (RLS) filter [FIG. 1(D)].

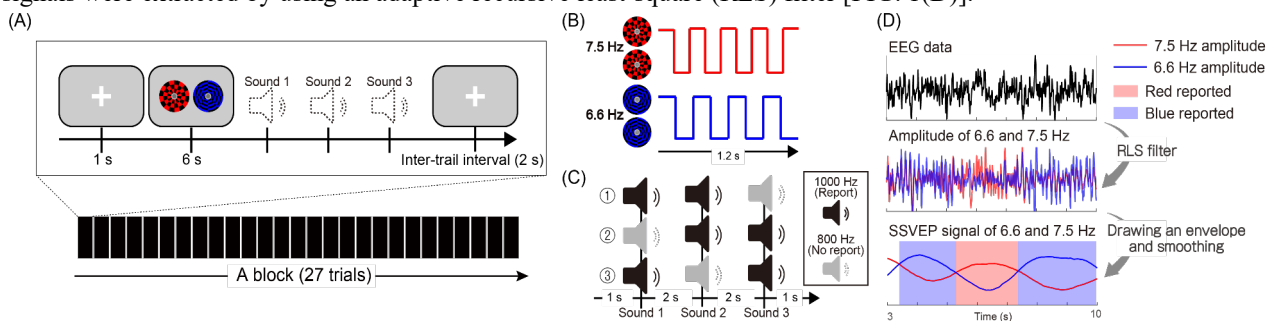


FIG. 1. (A) Schematic illustration of the task for a block. A participant conducted a total of 10 blocks. (B) Time-course modulation of checkerboard patterns. (C) Three timings on the measurement of perceived stimuli. The perceived stimulus was measured at two out of three timepoints for the calculation of the temporal Bell inequality. (D) Steps for SSVEP calculation using a 30-second binocular rivalry data. An adaptive RLS filter was applied to the raw EEG data in the top figure. In the middle figure, the extracted frequency-tagged amplitudes of 7.5 and 6.6 Hz were depicted. The bottom figure indicates that the frequency-tagged amplitude extracted by SSVEP was consistent with the subjective report.

### Reference

<sup>1</sup>H. Atmanspacher, and T. Filk, *J. Math. Psychol.* **54**, 314-321 (2010).

### Acknowledgement

This work was supported by JSPS KAKENHI JP20H05711 and MEXT Q-LEAP Grant Number JPMXS0120330644.

## X-ray absorption spectroscopy of a silicon phthalocyanine derivative, IR700, for X-ray excited photoimmunotherapy

Y. Izumi<sup>1</sup>, M. Ohara<sup>1</sup>, K. Fujii<sup>1</sup>, A. Yokoya<sup>1</sup>, R. Watanabe<sup>1</sup>, K. Nakagawa<sup>2</sup>, O. Inanami<sup>3</sup>, T. Taketsugu<sup>4</sup>, and M. Ogawa<sup>5</sup>

<sup>1</sup>Institute for Quantum Life Science, National Institutes for Quantum Science and Technology (QST)

<sup>2</sup>Graduate School of Engineering, The University of Tokyo

<sup>3</sup>Graduate School of Veterinary Medicine, Hokkaido University

<sup>4</sup>Faculty of Science, Hokkaido University

<sup>5</sup>Graduate School of Pharmaceutical Sciences, Hokkaido University

izumi.yudai@qst.go.jp

### Introduction

Photoimmunotherapy (PIT) has been recognized as one of the most promising methods in advanced cancer therapies [1]. A silicon phthalocyanine derivative (IR700) conjugated to a monoclonal antibody (mAb) targeting epidermal growth factor receptors of cancer membranes is used as a photosensitizing molecule. Irradiating the mAb-IR700-bound cancer cells with near-infrared (NIR) light, axial ligands of the IR700 are released. It makes the cell membranes brittle and, as a result, prompts cell death. Though the evidence clearly shows a strong potential of the PIT, the short penetration depth of NIR (a few centimeters) might be controversial when it is applied to deeply located tumors. We have focused on X-ray-induced core level excitations as alternative initiation probes owing to those long penetration depths. In this work, the reaction probability of the IR700 with X-rays was evaluated by measuring atom selective K-shell X-ray absorption spectra using a synchrotron radiation soft-X-ray beamline.

### Methods

Thin films of IR700 were prepared on gold plates by drying an aqueous solution of IR700 at room temperature. X-ray absorption spectroscopy of the films was performed in the BL23SU at SPring-8 in Japan. The absorption spectra were measured in the nitrogen, oxygen, and silicon K-edge energy regions, in which corresponding K-shell electrons were excited selectively. The optical absorption cross-section in each region was evaluated.

### Results and Discussion

The absorption cross-section of the oxygen K-shell resonance excitation  $\sigma_r$  (~536 eV) was almost two folds of that at the pre-edge region  $\sigma_p$  (~530 eV) in which the oxygen atoms were not excited (FIG. 1). It was larger than those of the nitrogen and silicon K-shell resonance excitations.

X-ray-induced bond breakages often occur in the vicinity of the excited atoms. Since the axial ligands and the phthalocyanine body of the IR700 are linked via oxygen atoms, the oxygen K-shell excitations could be effective to detach the axial ligands, similar to the NIR irradiations.

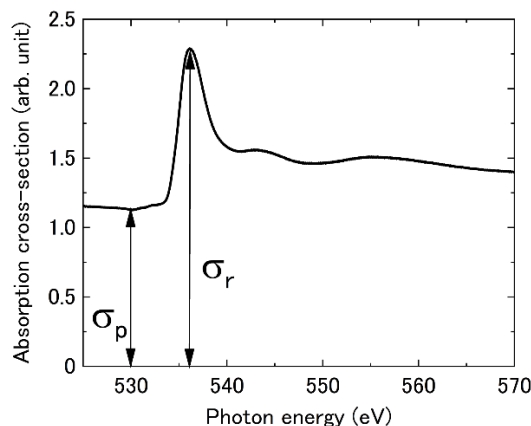


FIG. 1. X-ray absorption spectrum of the IR700 thin film in the oxygen K-edge energy region.

### Reference

<sup>1</sup>M. Kobayashi *et al.*, *ChemPlusChem*, **85**, 1959 (2020).

## Magnetically sensitive radical pairs in avian cryptochrome 4 proteins

Presenters: Jingjing Xu<sup>1</sup>, Siu Ying Wong<sup>2</sup>

<sup>1</sup>*Institute of Biology and Environmental Sciences, Carl-von-Ossietzky University Oldenburg,*

<sup>2</sup>*Department of Physics, Carl-von-Ossietzky Universität Oldenburg,*

*jingjing.xu@uni-oldenburg.de*

\*A list of authors and affiliations appears on the next page.

### Introduction

Migratory birds use the earth's magnetic field to navigate during their spectacular migratory journeys<sup>1</sup>. The avian magnetic compass was proposed to be based on quantum effects in radical pairs (RP) in cryptochrome (CRY) proteins<sup>2,3</sup>. Specifically, transfer of an electron along a chain of tryptophan residues to the photoexcited chromophore, flavin adenine dinucleotide (FAD), in CRY generates a spin-correlated flavin-tryptophan radical pair. An external magnetic field could alter the time-dependent fractions of RPs present in the singlet and triplet states and change the product yields of spin-selective RP chemical reactions<sup>4</sup>. However, there had been no experimental evidence showing a magnetic sensitivity of CRY proteins from any migratory bird.

### Method

Cryptochrome 4 proteins from the migratory European robin (*Erithacus rubecula*, *ErCRY4*) and non-migratory birds pigeon (*Columba livia*, *CiCRY4*) and chicken (*Gallus gallus*, *GgCRY4*) were produced using an *E. coli* expression system. Magnetic field effects on CRY4 proteins were measured optically using various spectroscopic techniques, including picosecond transient absorption spectroscopy, cavity ring-down spectroscopy, broadband cavity-enhanced absorption spectroscopy, and electron paramagnetic resonance.

### Results

A long-lived spin-correlated radical pair is formed via light-induced electron hopping along a tetrad of tryptophan residues to FAD in European robin CRY4 (FIG. 1A and 1B). *ErCRY4* is more sensitive to weak magnetic fields than the plant CRY given other factors being equal, e.g., pH7 and tryptophan-triad (FIG. 1C). Moreover, *ErCRY4* shows a more pronounced magnetic field effect than non-migratory pigeon and chicken CRY4s (FIG. 1D).

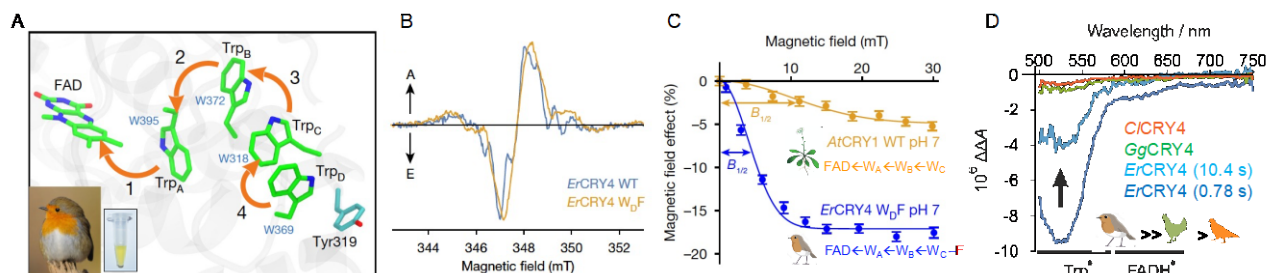


FIG. 1. A light-induced magnetically sensitive radical pair in cryptochrome proteins. A, Structural homology model of European robin CRY4 (*ErCRY4*) showing sequential electron transfer from tryptophan residues (Trp, W) to the FAD. Inset shows a robin and a CRY4 protein sample with FAD bound. B, Time-resolved X-band (9.75 GHz) electron paramagnetic resonance spectra of wild-type *ErCRY4* and the terminal tryptophan mutant (*W<sub>D</sub>F*) recorded at 1 °C, 0.5 μs after a 450-nm laser pulse. In the *ErCRY4 W<sub>D</sub>F* mutant, the fourth tryptophan was replaced by a redox-inactive phenylalanine residue to block the fourth electron transfer step. C, Comparison of magnetic field effects on *ErCRY4 W<sub>D</sub>F* and *Arabidopsis thaliana* cryptochrome (*AtCRY*).  $B_{1/2}$  is the intensity of a magnetic field that produces 50% of the overall magnetic field effect. D, Change in the optical absorbance of photoinduced radicals in three avian CRY4 samples induced by a 30-mT magnetic field. *ErCRY4* spectra are shown at two different times after the start of illumination.

### Conclusion:

Cryptochrome 4 from the European robin is magnetically sensitive *in vitro* and could be the long sought-after magnetic sensor in night-migratory songbirds.

### Reference

<sup>1</sup>H. Mouritsen, *Nature* **558**, 50-59 (2018).

<sup>2</sup>K. Schulten, et al., *Z. Phys. Chem.* **111**, 1-5 (1978).

<sup>3</sup>T. Ritz, et al., *Biophys. J.*, **78**, 707-718 (2000)

<sup>4</sup>P. J. Hore & H. Mouritsen, *Annu. Rev. Biophys.* **45**, 299-344 (2016),

## **Authors:**

Jingjing Xu<sup>1+</sup>, Lauren E. Jarochoa<sup>2+</sup>, Tilo Zollitsch<sup>2+</sup>, Marcin Konowalczyk<sup>3+</sup>, Kevin B. Henbest<sup>2,3+</sup>, Sabine Richert<sup>4+</sup>, Matthew J. Golesworthy<sup>3+</sup>, Jessica Schmidt<sup>1</sup>, Victoire Déjean<sup>3</sup>, Daniel J. C. Sowood<sup>2</sup>, Marco Bassetto<sup>1,2</sup>, Jiatae Luo<sup>2</sup>, Jessica R. Walton<sup>2</sup>, Jessica Fleming<sup>2</sup>, Yujing Wei<sup>2</sup>, Tommy L. Pitcher<sup>3</sup>, Gabriel Moise<sup>3</sup>, Maike Herrmann<sup>1</sup>, Hang Yin<sup>5</sup>, Haijia Wu<sup>6</sup>, Rabea Bartölke<sup>1</sup>, Stefanie J. Käsehagen<sup>1</sup>, Simon Horst<sup>1</sup>, Glen Dautaj<sup>1</sup>, Patrick D. F. Murton<sup>2</sup>, Angela S. Gehrckens<sup>2</sup>, Yogarany Chelliah<sup>7,8</sup>, Joseph S. Takahashi<sup>7,8</sup>, Karl-Wilhelm Koch<sup>6,9</sup>, Stefan Weber<sup>4</sup>, Ilia A. Solov'yov<sup>9,10\*</sup>, Can Xie<sup>11\*</sup>, Stuart R. Mackenzie<sup>2\*</sup>, Christiane R. Timmel<sup>3,12\*</sup>, Henrik Mouritsen<sup>1,9\*</sup>, P. J. Hore<sup>2\*</sup>

<sup>1</sup>AG Neurosensory Sciences/Animal Navigation, Institut für Biologie und Umweltwissenschaften, Carl-von-Ossietzky Universität Oldenburg, 26111 Oldenburg, Germany

<sup>2</sup>Department of Chemistry, University of Oxford, Physical and Theoretical Chemistry Laboratory, Oxford OX1 3QZ, UK

<sup>3</sup>Department of Chemistry, University of Oxford, Inorganic Chemistry Laboratory, Oxford OX1 3QR, UK

<sup>4</sup>Institut für Physikalische Chemie, Albert-Ludwigs-Universität Freiburg, 79104 Freiburg, Germany

<sup>5</sup>Department of Medicinal Chemistry and Molecular Pharmacology, Purdue University, West Lafayette, IN 47907, USA

<sup>6</sup>Division of Biochemistry, Department of Neuroscience, Carl-von-Ossietzky Universität Oldenburg, DE-26111 Oldenburg, Germany

<sup>7</sup>Department of Neuroscience, University of Texas Southwestern Medical Center, Dallas, TX 75390-9111, USA

<sup>8</sup>Howard Hughes Medical Institute, University of Texas Southwestern Medical Center, Dallas, TX 75390-9111, USA

<sup>9</sup>Research Centre for Neurosensory Science, University of Oldenburg, 26111 Oldenburg, Germany

<sup>10</sup>Department of Physics, Carl-von-Ossietzky Universität Oldenburg, 26111 Oldenburg, Germany

<sup>11</sup>CAS Key Laboratory of High Magnetic Field and Ion Beam Physical Biology, High Magnetic Field Laboratory, Hefei Institutes of Physical Science, Chinese Academy of Sciences, Hefei, Anhui 230031, PR China

<sup>12</sup>Centre for Advanced Electron Spin Resonance (CAESR), Department of Chemistry, University of Oxford, Oxford OX1 3QR, UK